SUPPLEMENTARY MATERIAL

Boosting the Sustainable Recycling of Spent Lithium-ion Batteries through Mechanochemistry

Shubin Wang[a]‡, Shuxuan Yan[b]‡, Zihao Chen[c,d], Yudie Ou[b], Binod Mahara[c,d], Xiangping Chen[c,d], Ying Yang[b] and Tao Zhou[b*]*

[a] State Environmental Protection Key Laboratory of Environmental Pollution Health Risk Assessment, South China Institute of Environmental Sciences, Ministry of Ecology and Environment (MEE), Guangzhou 510655, P.R. China;

[b] Hunan Provincial Key Laboratory of Chemical Power Sources, College of Chemistry and Chemical Engineering, Central South University, Changsha 410083, P.R. China;

[c] College of Chemistry and Chemical Engineering, Hunan Normal University, Changsha 410081, P.R. China.

[d] National & Local Joint Engineering Laboratory for New Petro-chemical Materials and Fine Utilization of Resources, Hunan Normal University, Changsha 410081, P.R. China.

Table and Text legend

Table S1 XPS spectral peak sites (eV) and regions (%) fitting of Fe 2p in products with different milling rotation speeds.

Table S2 XPS spectral peak sites (eV) and regions (%) fitting of Ni 2p in products with different milling rotation speeds.

Table S3 XPS spectral peak sites (eV) and regions (%) fitting of Co 2p in products with different milling rotation speeds.

Table S4 XPS spectral peaks of Mn 3s in products with different milling rotation speeds.

Table S5 Thermodynamic data for the related species at 298.15 K.

Table S6 Gibbs free energy values ($\Delta_r G_m$) for Eq. (4)-(15) at 298.15 K.

Table S7 Lattice parameters (a, b, c) and unit cell volume (V).

Table S8 Preprocessing and Critical Materials (CM) Recovery.

Table S9 Material requirements (kg) to recycle 1 kg of spent batteries through different recycling technologies. (N = No need).

Table S10 Energy requirements (MJ) to recycle 1 kg of spent batteries through different recycling technologies. (N = No need).

Table S11 Life-cycle environmental impacts of different recycling methods (per kg feedstock processed).

Table S12 Horizontal comparisons using multi-indicator evaluation systems of different technologies.

Text S1 DFT calculations.

Figure legend

Figure S1 The flow chart of proposed green route for recovery of valuable metals from spent LIBs.

Figure S2 Pore width distribution of samples before and after MR.

Figure S3 XPS spectra of P 2p in products without and after MR.

Figure S4 Schematic Diagram of Product Properties.

Figure S5 Effect of (a) rotation speed and (b) milling time on the water leaching efficiency of milling product.

Figure S6 Effect of milling rotation speed on the water leaching efficiency of milling products. (Factorial experiments, other than the exploratory factor, were conditioned on solid-liquid ratio: 5 g/L, temperature: 90 °C, time: 60 min, ball powder ratio: 50: 1, rotation speed: 750 rpm, milling time: 7 h).

Figure S7 Leaching efficiency of samples at different acid concentrations (a) without and (b) after MR.

Figure S8 Effect of (a) ball powder ratio, (b) leaching time, and (c) molar ratio of LFP: NCM on leaching efficiency.

Figure S9 Effect of (a) rotation speed, and (b) temperature on leaching efficiency.

Figure S10 Comparison of leaching effect of different samples before and after MR:

(a) NCM811, (b) NCM333 (b), and (c) LCO.

Figure S11 Structural diagrams of NCM, CoO, MnO, NiO, LFP, FP, and Li_2O.

Figure S12 XRD pattern of recovered Li_2CO_3.

Figure S13 XRD pattern water leaching residues.

Figure S14 SEM-EDS images of leaching residues after roasting at 600°C for 20 min.

Figure S15 SEM-EDS images of leaching residues after roasting at 600^{o}C for 20 min.

Figure S16 XPS spectra of (a) Fe2p and (b) P 2p of leaching residues after roasting at 600^{o}C for 20 min.

Figure S17 configurations of tetrahedral PO_4 in LFP and FP.

Figure S18 (a) XRD pattern and (b) SEM image of the $Ni_{0.5}Co_{0.2}Mn_{0.3}(OH)_2$.

Figure S19 Schematic of Pyro recycling.

Figure S20 Schematic of Hydro recycling.

Figure S21 Schematic of this work.

Table S1 XPS spectral peak sites (eV) and regions (%) fitting of Fe 2p in products with different milling rotation speeds.

Rotational speed (rpm)		Fe $2p_{3/2}$				Fe $2p_{1/2}$				Content (*wt.*%)	
		Peak1 Fe^{2+}	Peak2 Fe^{3+}	S1 Fe^{2+}	S2 Fe^{3+}	Peak3 Fe^{2+}	Peak4 Fe^{3+}	S3 Fe^{2+}	S4 Fe^{3+}	Fe^{2+}	Fe^{3+}
0	Sites (eV)	710.33	711.75	713.09	715.82	723.67	725.23	726.78	729.62	77.31	22.69
	Regions (%)	14.90	4.37	11.40	14.90	17.81	5.23	13.63	17.76		
450	Sites (eV)	710.71	712.11	715.18	719.14	723.51	725.51	728.41	732.94	46.67	53.33
	Regions (%)	13.67	15.62	10.28	5.98	16.34	18.67	12.28	7.15		
550	Sites (eV)	710.43	711.79	714.67	718.75	723.23	725.17	727.97	732.55	38.25	61.75
	Regions (%)	11.29	18.22	10.73	5.31	13.49	21.78	12.82	6.35		
650	Sites (eV)	710.30	711.64	714.44	718.65	723.10	725.05	727.97	732.45	36.75	63.25
	Regions (%)	10.08	18.01	10.79	5.96	12.89	21.52	12.90	7.13		
750	Sites (eV)	710.06	711.54	714.41	718.53	722.86	725.95	727.92	732.33	33.87	66.13
	Regions (%)	10.01	19.54	10.48	5.52	11.96	23.35	12.53	6.61		
850	Sites (eV)	709.95	711.27	714.08	718.40	722.75	724.65	727.52	732.20	35.42	64.58
	Regions (%)	10.48	19.10	10.88	5.09	12.52	22.83	13.00	6.09		

Notes: $C(Fe^{2+}) = (S_{P1} + S_{P3})/(S_{P1} + S_{P2} + S_{P3} + S_{P4})$, $C(Fe^{3+}) = (S_{P2} + S_{P4})/(S_{P1} + S_{P2} + S_{P3} + S_{P4})$,

$I(Fe^{3+}/Fe^{2+}) = C(Fe^{3+})/C(Fe^{2+})$

Table S2 XPS spectral peak sites (eV) and regions (%) fitting of Ni 2p in products with different milling rotation speeds.

Rotational speed (rpm)		Ni $2p_{3/2}$				Ni $2p_{1/2}$			Content (*wt.*%)	
		Peak 1 Ni^{2+}	Peak 2 Ni^{3+}	S1 Ni^{2+}	S2 Ni^{3+}	Peak 3 Ni^{2+}	Peak 4 Ni^{3+}	S3 Ni^{2+}	Fe^{2+}	Fe^{3+}
0	Sites (eV)	855.05	856.81	861.22	864.49	872.54	875.22	879.63	68.04	31.96
	Regions (%)	21.01	9.87	14.42	3.14	23.9	11.23	16.43		
450	Sites (eV)	855.4	857.22	861.63	865.38	873.93	875.63	879.5	71.20	28.80
	Regions (%)	18.64	7.54	21.18	2.94	20.02	7.61	23.96		
550	Sites (eV)	855.5	857.35	861.43	865.17	873.07	875.76	879.81	71.67	28.33
	Regions (%)	20.49	8.1	16.54	3.48	23.31	9.32	18.85		
650	Sites (eV)	855.27	857.1	861.16	864.42	872.83	875.51	879.44	72.97	27.03
	Regions (%)	19.9	7.37	18.46	2.03	22.64	8.59	21		
750	Sites (eV)	855.22	857.65	861.15	864.8	872.85	876.06	879.45	74.61	25.39
	Regions (%)	22.72	7.73	14.95	2.75	25.85	8.96	17.03		
850	Sites (eV)	855.04	857.01	861.08	864.6	872.82	875.42	879.49	72.41	27.59
	Regions (%)	20.58	7.84	17.15	2.52	23.43	8.93	19.54		

Notes: $C(Ni^{2+}) = (S_{P1} + S_{P3})/(S_{P1} + S_{P2} + S_{P3} + S_{P4})$, $C(Ni^{3+}) = (S_{P2} + S_{P4})/(S_{P1} + S_{P2} + S_{P3} + S_{P4})$, $I(Ni^{2+}/Ni^{3+}) = C(Ni^{2+})/C(Ni^{3+})$

Table S3XPS spectral peak sites (eV) and regions (%) fitting of Co 2p in products with different milling rotation speeds.

Rotational speed (rpm)		Co $2p_{3/2}$				Co $2p_{1/2}$				Content (*wt.*%)	
		Peak1 Co^{3+}	Peak2 Co^{2+}	S1 Co^{3+}	S2 Co^{2+}	Peak3 Co^{3+}	Peak4 Co^{2+}	S3 Co^{3+}	S4 Co^{2+}	Co^{3+}	Co^{2+}
0	Sites (eV)	779.94	780.78	781.37	789.84	795.01	796.09	797.16	804.96	70.07	29.93
	Regions (%)	17.04	7.42	19.96	4.97	17.56	7.50	20.46	5.09		
450	Sites (eV)	780.51	782.78	786.05	789.44	795.2	797.53	801.84	805.23	58.88	41.12
	Regions (%)	17.29	12.09	11.96	8.04	17.75	12.38	12.26	8.24		
550	Sites (eV)	780.3	782.56	785.83	789.38	794.99	797.25	801.62	805.17	56.74	43.26
	Regions (%)	16.01	12.22	12.54	8.61	16.43	12.51	12.85	8.83		
650	Sites (eV)	780.05	782.12	785.43	788.96	794.74	797.1	801.22	804.75	50.94	49.06
	Regions (%)	13.62	13.13	13.62	9.01	13.98	13.45	13.96	9.24		
750	Sites (eV)	779.71	780.75	785.07	788.47	794.4	796.81	800.86	804,26	31.95	68.05
	Regions (%)	8.1	17.26	14.24	9.8	8.3	17.67	14.59	10.05		
850	Sites (eV)	779.74	781.64	785.05	788.45	794.43	796.833	800.84	804.24	40.49	59.51
	Regions (%)	10.44	15.38	14.73	8.82	10.74	15.75	15.1	9.05		

Notes: $C(Co^{3+}) = (S_{P1} + S_{P3})/(S_{P1} + S_{P2} + S_{P3} + S_{P4})$, $C(Co^{2+}) = (S_{P2} + S_{P4})/(S_{P1} + S_{P2} + S_{P3} + S_{P4})$,

$I(Co^{2+}/Co^{3+}) = C(Co^{2+})/C(Co^{3+})$

Table S4 XPS spectral peaks of Mn 3s in products with different milling rotation speeds.

Rotational speed (rpm)	Sites (eV)		ΔE_{3s} (eV)	AOS
	Peak1	Peak2		
0	84.27	89.06	4.79	3.59
450	83.41	88.45	5.04	3.27
550	83.07	88.19	5.12	3.17
650	83.10	88.31	5.21	3.05
750	82.72	88.62	5.90	2.18
850	82.71	88.27	5.56	2.61

Table S5 Thermodynamic data for the related species at 298.15 K.

Substance	$\Delta_f G_m^\theta$ (kJ/mol)	Ref.	Substance	$\Delta_f G_m^\theta$ (kJ/mol)	Ref.
$LiFePO_4$	-1480.97	[1]	$FePO_4$	-1179.3	[1]
$LiNi_{0.5}Co_{0.2}Mn_{0.3}O_2$	-640.04	[2]	FeO	-251.4	[3]
CoO	-214.00	[3]	$LiCoPO_4$	-5660.10	[4]
Li_2O	-561.20	[3]	$LiNiPO_4$	-5881.77	[4]
Co_3O_4	-774.00	[3]	$LiMnPO_4$	-5096.46	[4]
Mn_3O_4	-1283.2	[3]	H_2SO_4	-689.90	[3]
Ni_2O_3	-469.74	[5, 6]	$CoSO_4$	-782.40	[3]
MnO	-362.9	[3]	Li_2SO_4	-1331.20	[3]
NiO	-211.7	[3]	$NiSO_4$	-790.30	[3]
Li_3PO_4	-2127.45	HSC 6.0	$MnSO_4$	-972.80	[3]
Fe_2O_3	-742.2	[3]	H_2O	-237.14	[3]

Table S6 Gibbs free energy values ($\Delta_r G_m$) for Eqs. (4)-(15) at 298.15 K.

No.	Reaction equation	$\Delta_r G_m$ (kJ/mol)
(4)	$10LiFePO_4+10LiNi_{0.5}Co_{0.2}Mn_{0.3}O_2=10FePO_4+3MnO+5NiO+2CoO+10Li_2O$	1229.9
(5)	$10LiFePO_4+10LiNi_{0.5}Co_{0.2}Mn_{0.3}O_2+20H_2SO_4=10FePO_4+2CoSO_4+10Li_2SO_4+5NiSO_4+3MnSO_4+20H_2O$	-3274.4
(6)	$8LiFePO_4+120LiNi_{0.5}Co_{0.2}Mn_{0.3}O_2=8FePO_4+12Mn_3O_4+30Ni_2O_3+8Co_3O_4+64Li_2O+3O_2$	7618.76
(7)	$2LiFePO_4+Co_3O_4=2FePO_4+3CoO+Li_2O$	174.14
(8)	$2LiFePO_4+Mn_3O_4=2FePO_4+3MnO+Li_2O$	236.64
(9)	$2LiFePO_4+Ni_2O_3=2FePO_4+2NiO+Li_2O$	88.48
(10)	$30LiFePO_4+30LiNi_{0.5}Co_{0.2}Mn_{0.3}O_2=20Li_3PO_4+10FePO_4+6CoO+9MnO+5NiO+10Fe_2O_3$	-3742.3
(11)	$60LiFePO_4+120LiNi_{0.5}Co_{0.2}Mn_{0.3}O_2=60Li_3PO_4+12Mn_3O_4+30Ni_2O_3+8Co_3O_4+8Fe_3O_4+19O_2$	-5615.4
(12)	$3LiFePO_4+Co_3O_4=Li_3PO_4+3CoO+2FePO_4+FeO$	-162.54
(13)	$3LiFePO_4+Mn_3O_4=Li_3PO_4+3MnO+2FePO_4+FeO$	-100.04
(14)	$3LiFePO_4+Ni_2O_3=Li_3PO_4+2NiO+2FePO_4+FeO$	-248.2
(15)	$10LiFePO_4+10LiNi_{0.5}Co_{0.2}Mn_{0.3}O_2=2LiCoPO_4+5LiNiPO_4+3LiMnPO_4+5Fe_2O_3+5Li_2O$	-41325.33

Table S7 Lattice parameters (a, b, c) and unit cell volume (V).

Materials	a/Å	b/Å	c/Å	V/Å^3
$LiFePO_4$	10.42233	6.06186	4.74113	299.538459
$LiNi_{1/3}Co_{1/3}Mn_{1/3}O_2$	2.94763	2.94763	14.48677	109.005722
$FePO_4$	5.15897	5.15897	11.47868	264.574758
NiO	2.97764	2.97764	2.97764	18.668089
CoO	3.00037	3.00037	3.00037	19.098898
MnO	3.19334	3.19334	3.19334	23.025998
Li_2O	3.26613	3.26613	3.26613	24.636770

Table S8 Preprocessing and Critical Materials (CM) Recovery.

Feedstock chemistry	Feedstock type	Feedstock tonnage (tonne/yr)	Geographic location
S-NCM	End-of-life battery: cell	1580	China
S-LFP	End-of-life battery: cell	1000	China

Note: Preprocessed feedstock composition: NCM523-27.6%，LFP-17.7%，Graphite-25.1%，Carbon black-0.9%，Binder: PVDF-0.9%，Copper-8.6%，Aluminum-5.5%。

Table S9 Material requirements (kg) to recycle 1 kg of spent batteries through different recycling technologies. (N = No need).

	Pyrometallurgy	Hydrometallurgy	This work
Limestone	0.2	N	N
Sand	0.31	N	N
Sulfuric Acid	0.33	1.04	0.78
Lime	0.076	0.001	N
Hydrogen Peroxide	N	0.07	N
Sodium Hydroxide	N	0.63	N
Soda Ash	N	0.29	N

Table S10 Energy requirements (MJ) to recycle 1 kg of spent batteries through different recycling technologies. (N = No need).

	Pyrometallurgy	Hydrometallurgy	This work
Diesel	0.60	0.60	3
Natural gas	0.20	1.81	1.6
Electricity	1.12	0.90	10

Table S11 Life-cycle environmental impacts of different recycling methods (per kg feedstock processed).

Feedstock chemistry	Pyrometallurgy	Hydrometallurgy	This work
Cost	5.79	4.81	2.14
Energy use in MJ			
Total Energy	4.38	23.72	30.17
Fossil fuels	3.83	21.75	25.62
Coal	2.47	8.25	18.73
Natural gas	0.54	14.47	3.15
Petroleum	0.82	4.23	3.74
Water use in gallon	1.51	3.41	5.33
Total emissions in g			
VOC	0.07	0.28	0.36
CO	0.27	1.18	1.42
NO_x	0.68	2.18	3.67
PM10	0.07	0.21	0.40
PM2.5	0.05	0.15	0.24
SO_x	0.93	2.23	3.56
BC	0.01	0.03	0.07
OC	0.01	0.04	0.04
CH_4	0.54	3.57	3.75
N_2O	0.01	0.03	0.06
CO_2	1643.96	1754.79	2231.74
CO_2 (w/ C in VOC & CO)	1644.60	1757.51	2235.08
GHGs	1662.62	1873.32	2361.99

Revenue ($)	3.56	4.76	11.02
Profit ($)	-2.23	-0.05	8.87

Table S12 Horizontal comparisons using multi-indicator evaluation systems of different technologies.

	Pyrometallurgy	Hydrometallurgy	This work
Energy intensity	Medium	Low	Medium
Carbon emissions	Medium	Medium	Medium
Waste solid	High	Medium	Low
Waste water	Low	High	Low
Waste gas	High	Low	Low
Process complexity	Simplicity	Complexity	Simplicity
Recovery rate	Low	High	High
Profit	Low	Low	High

Text S1 DFT calculations.

The calculations employed a projector-augmented wave (PAW) pseudopotential for core electrons, with a 500-eV cutoff energy for valence electrons, and the Perdew–Burke–Ernzerhof (PBE) generalized gradient approximation (GGA) for the exchange–correlation potential. Structural relaxations were carried out until the force and energy convergence thresholds were below 0.02 eV/Å and 10^{-5} eV, respectively. The Monkhorst–Pack k-point meshes were set as follows: 10 × 10 × 10 for Li_2O, CoO, MnO, and NiO; 9 × 9 × 2 for $FePO_4$ (FP); 3 × 5 × 7 for LFP; and 12 × 12 × 12 for $LiNi_{1/3}Co_{1/3}Mn_{1/3}O_2$ (NCM111).

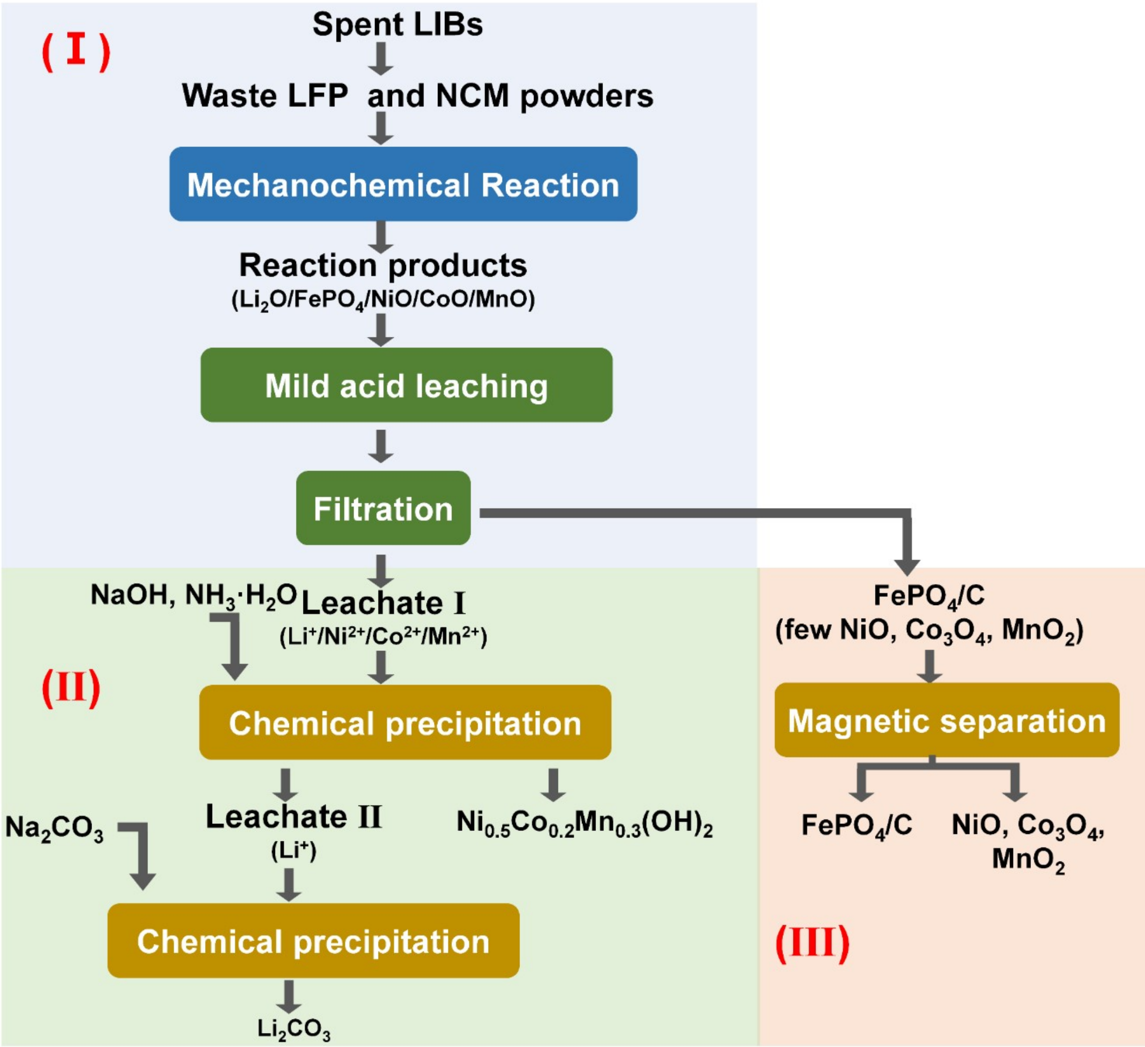

Figure S1 The flow chart of proposed green route for recovery of valuable metals from spent LIBs.

The process can be divided into three parts: part (I): Experimental process of mechanochemical reaction and stoichiometric acid leaching for recovering different cathodes from spent LIBs, in which pretreatments include discharging, dismantling, and exfoliation; part (II): Separation and recovery of valuable metals compo; part (III): Recovery of $FePO_4$.

Operators need to take precautions during the pretreatment process, as harmful components of the electrolyte, such as $LiPF_6$, can quickly decompose into LiF and PF_5. The gaseous PF_5

can be absorbed by specific adsorbents and the solid LiF will usually flow into the slag due to its high melting point (848 ^{o}C) and boiling point (1681 ^{o}C).

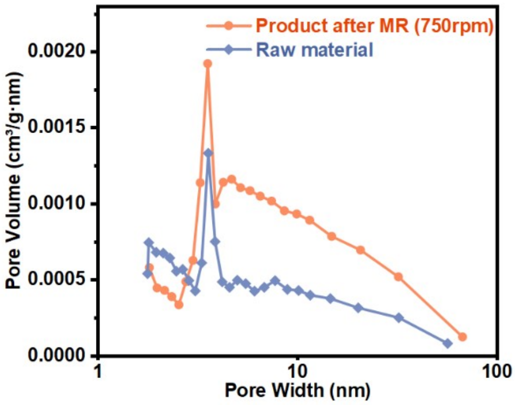

Figure S2 Pore width distribution of samples before and after MR.

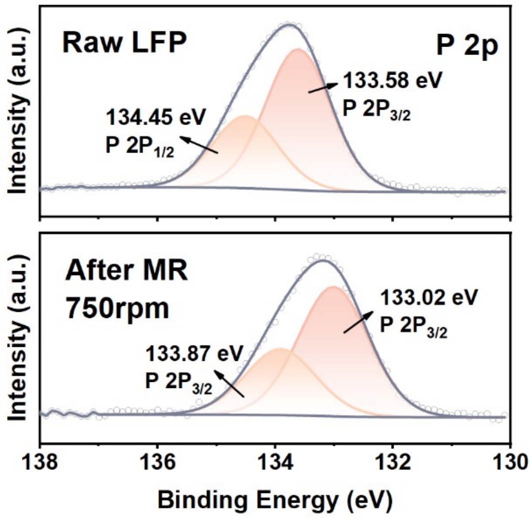

Figure S3 XPS spectra of P 2p in products without and after MR.

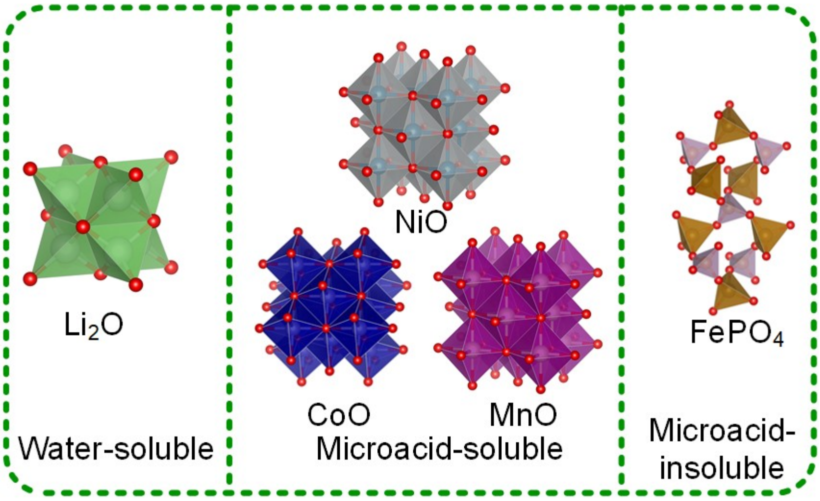

Figure S4 Schematic Diagram of Product Properties.

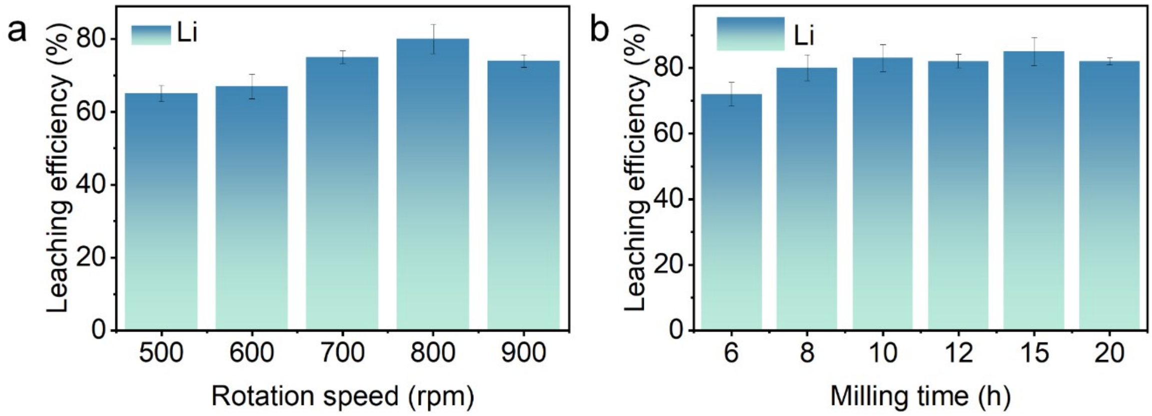

Figure S5 Effect of (a) rotation speed and (b) milling time on the water leaching efficiency of milling product.

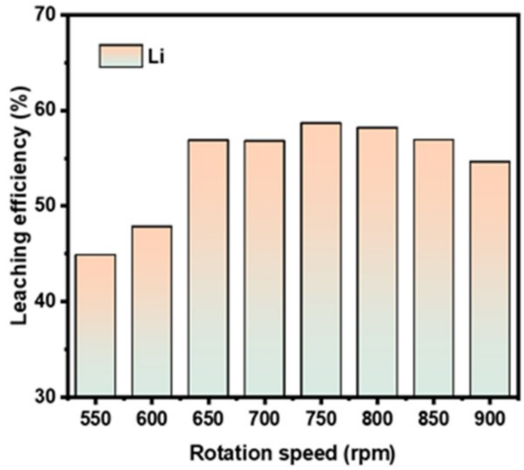

Figure S6 Effect of milling rotation speed on the water leaching efficiency of milling products. (Factorial experiments, other than the exploratory factor, were conditioned on solid-liquid ratio: 5 g/L, temperature: 90 °C, time: 60 min, ball powder ratio: 50: 1, rotation speed: 750 rpm, milling time: 7 h).

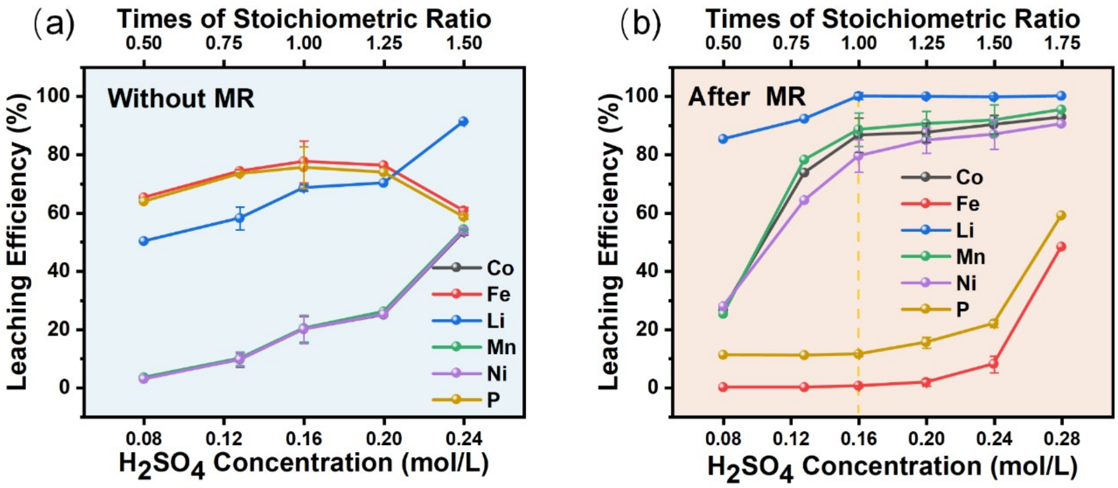

Figure S7 Leaching efficiency of samples at different acid concentrations (a) without and (b) after MR.

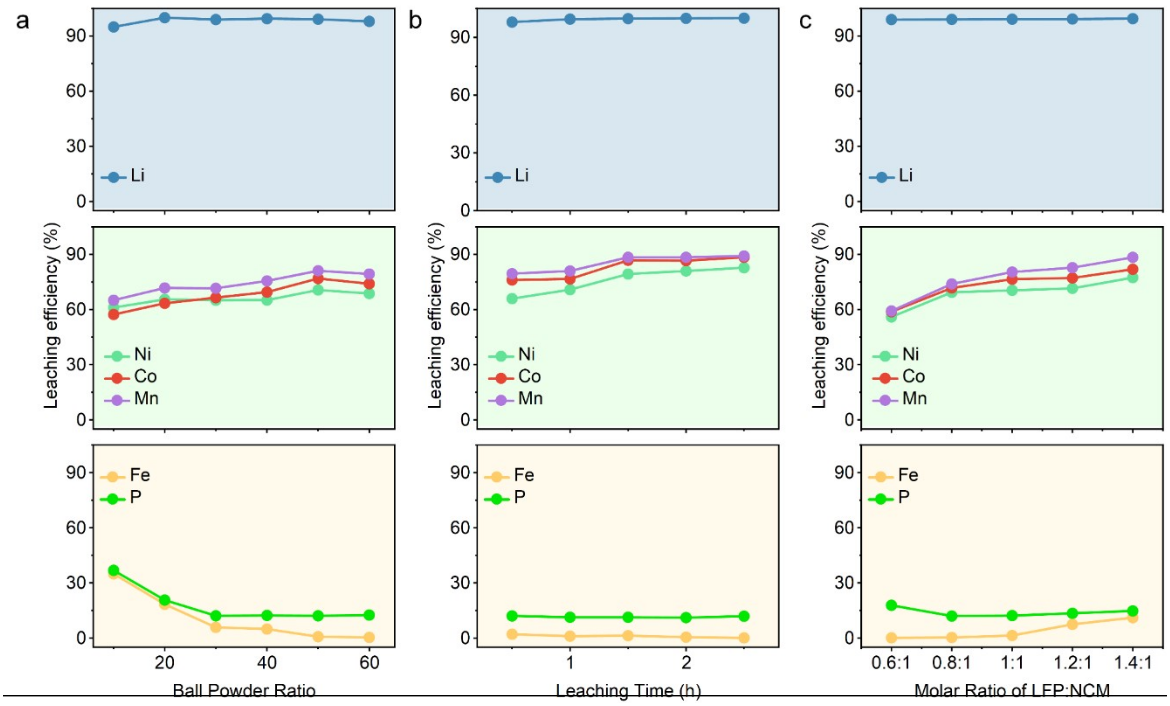

Figure S8 Effect of (a) ball powder ratio, (b) leaching time, and (c) molar ratio of LFP: NCM on leaching efficiency.

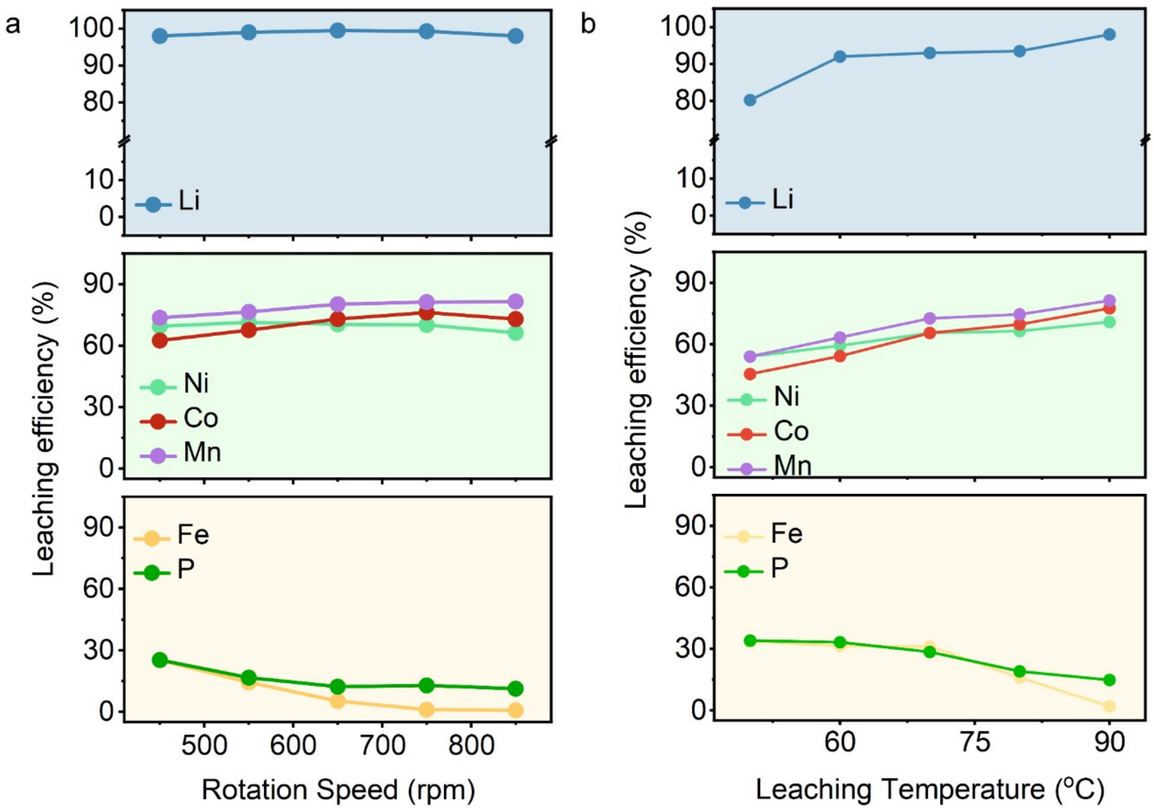

Figure S9 Effect of (a) rotation speed, and (b) temperature on leaching efficiency.

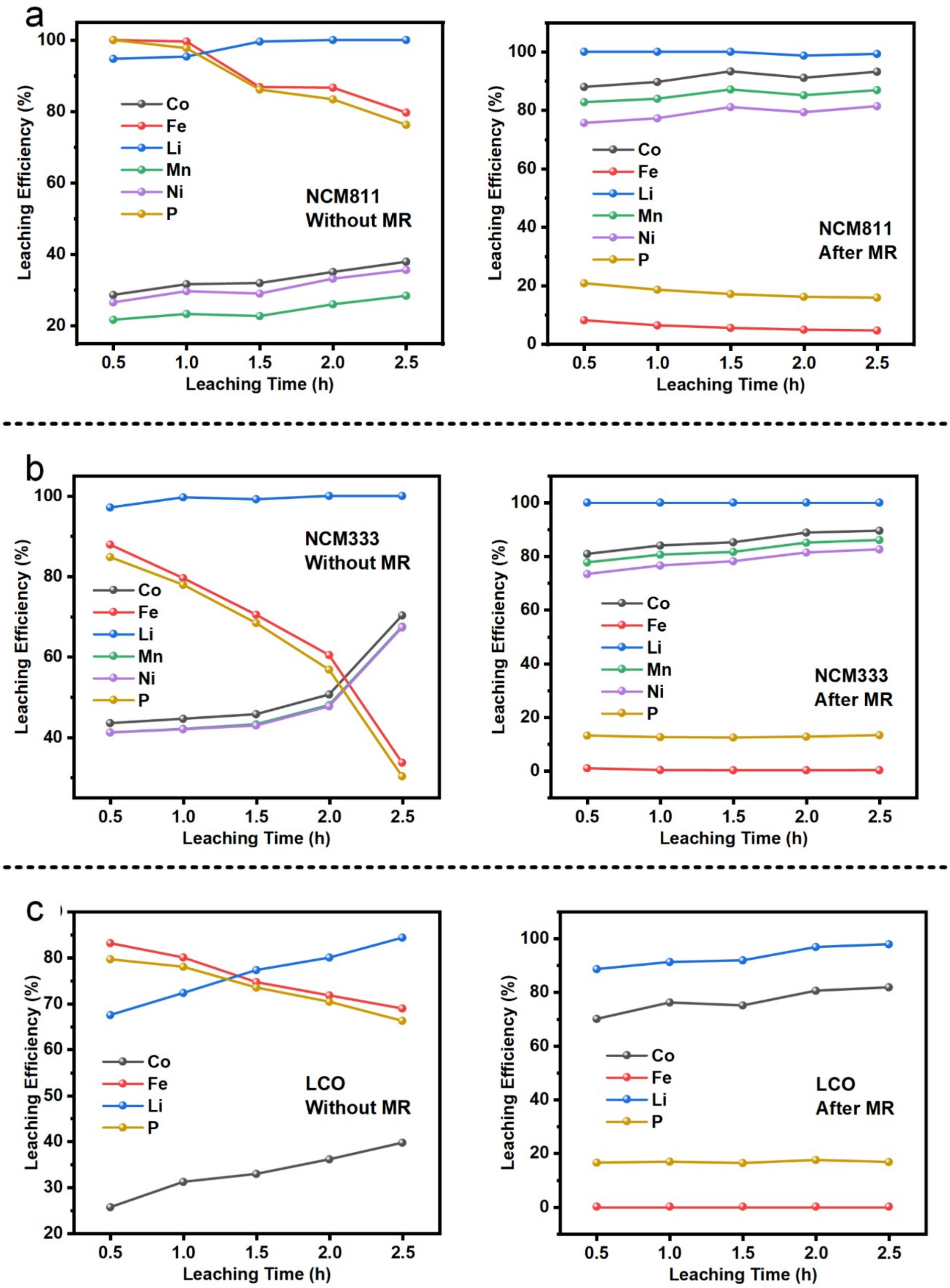

Figure S10 Comparison of leaching effect of different samples before and after MR: (a) NCM811, (b) NCM333 (b), and (c) LCO.

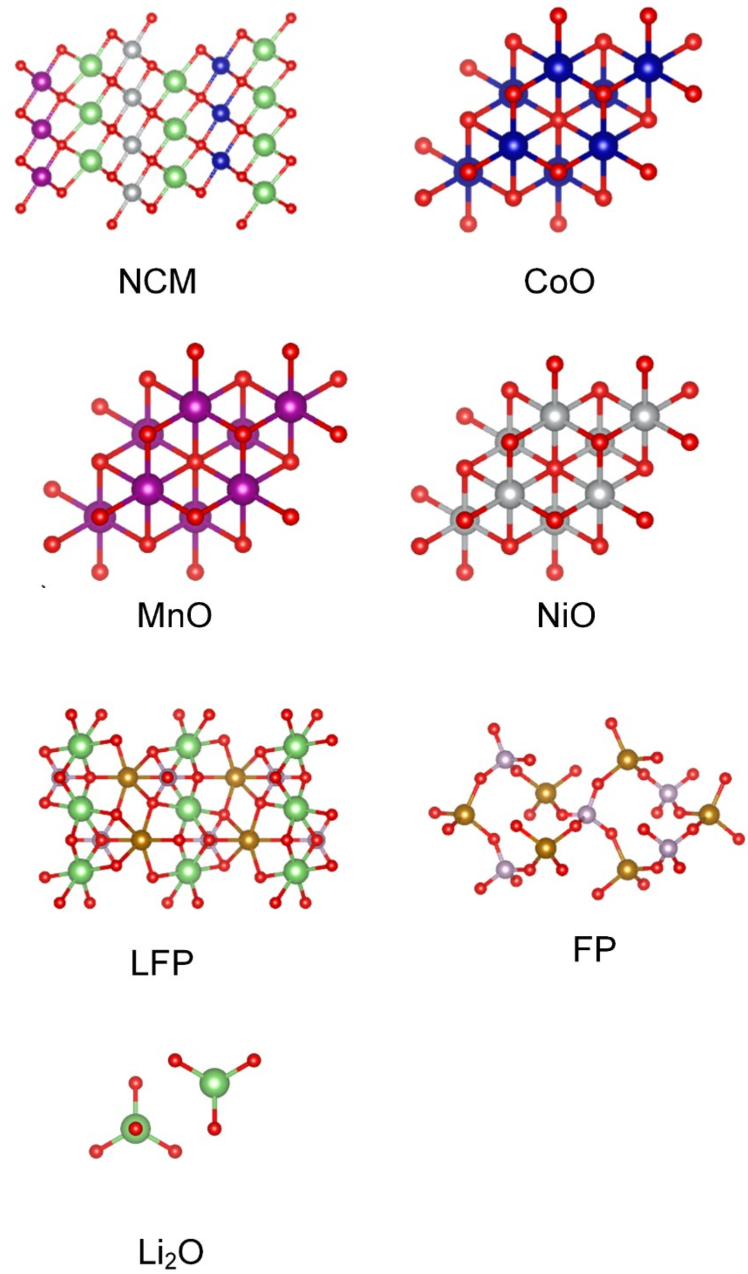

Figure S11 Structural diagrams of NCM, CoO, MnO, NiO, LFP, FP, and Li_2O.

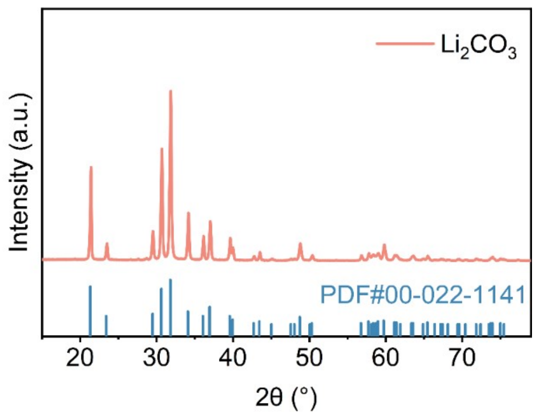

Figure S12 XRD pattern of recovered Li_2CO_3.

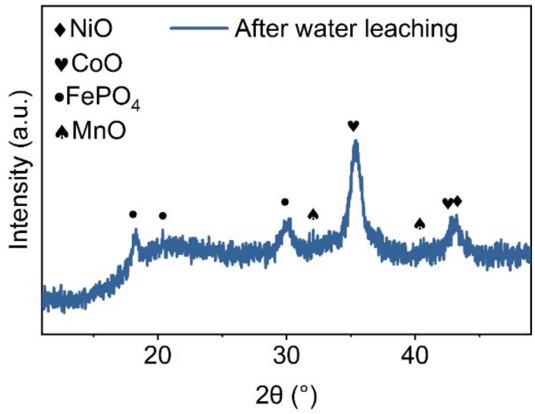

Figure S13 XRD pattern water leaching residues.

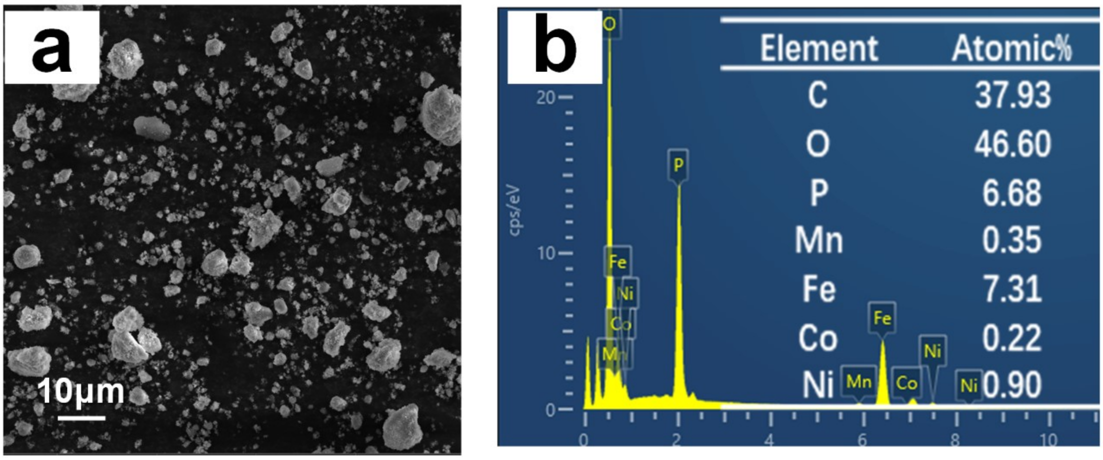

Figure S14 SEM-EDS images of leaching residues after roasting at 600°C for 20 min.

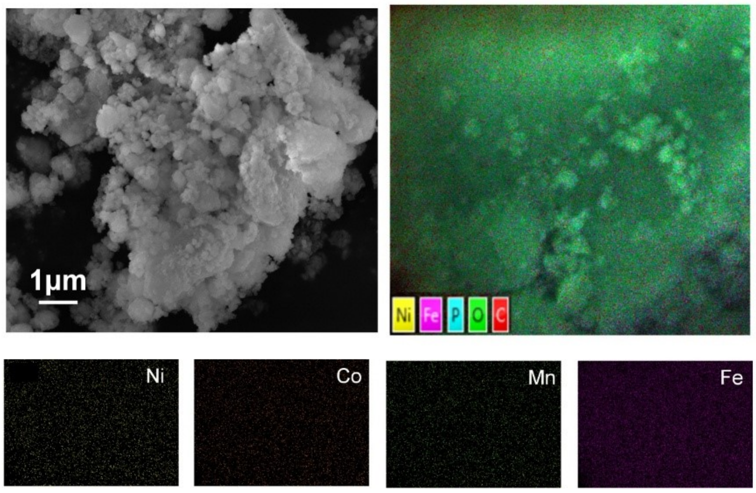

Figure S15 SEM-EDS images of leaching residues after roasting at 600^{o}C for 20 min.

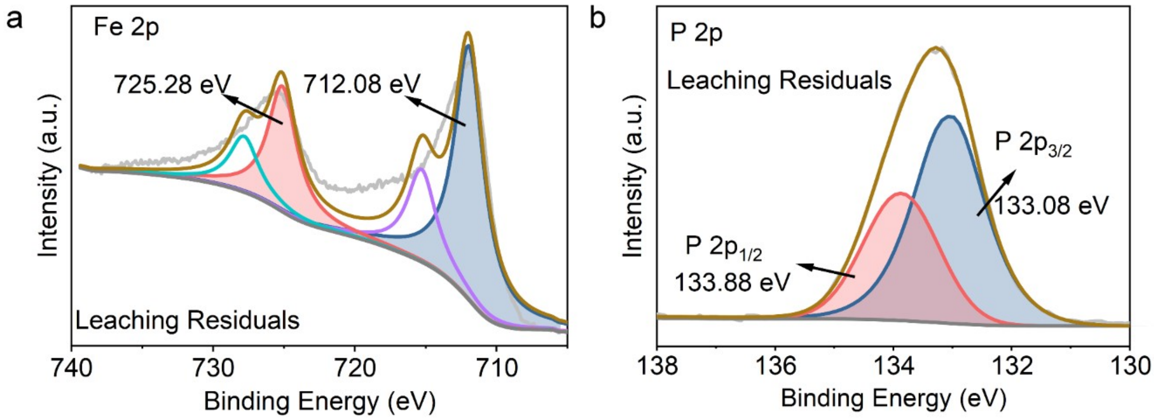

Figure S16 XPS spectra of (a) Fe2p and (b) P 2p of leaching residues after roasting at 600^{o}C for 20 min.

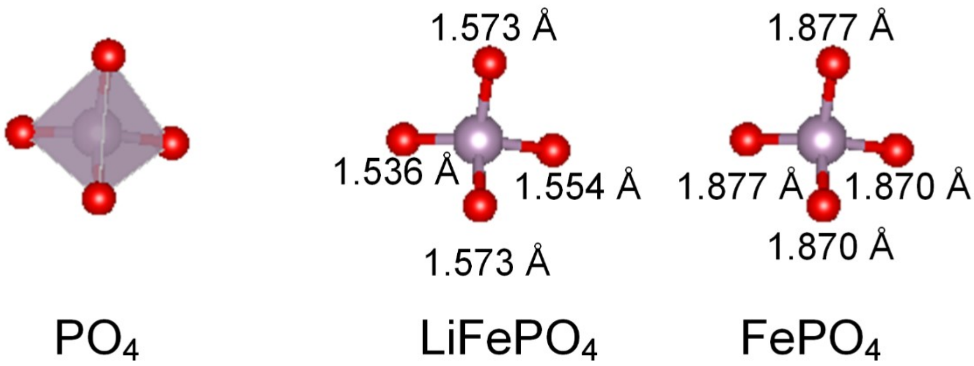

Figure S17 configurations of tetrahedral PO_4 in LFP and FP.

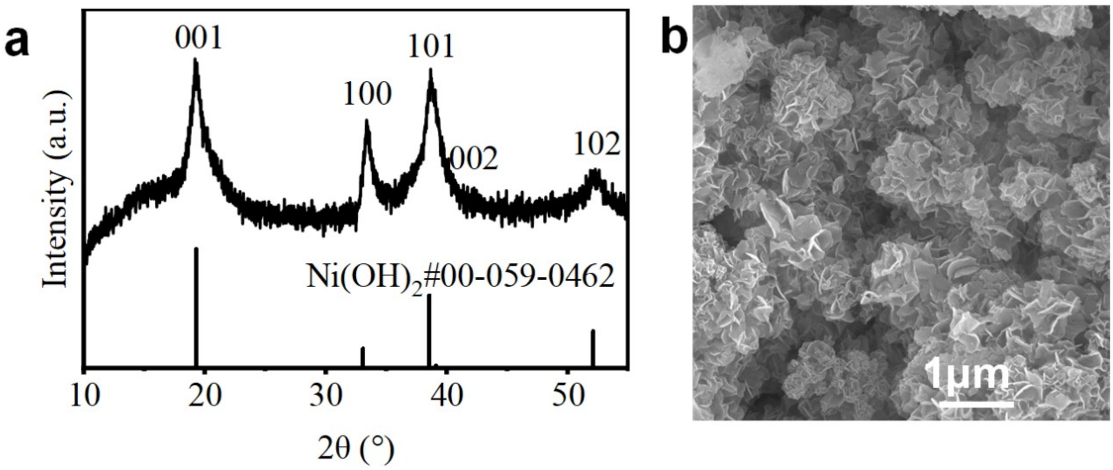

Figure S18 (a) XRD pattern and (b) SEM image of the $Ni_{0.5}Co_{0.2}Mn_{0.3}(OH)_2$.

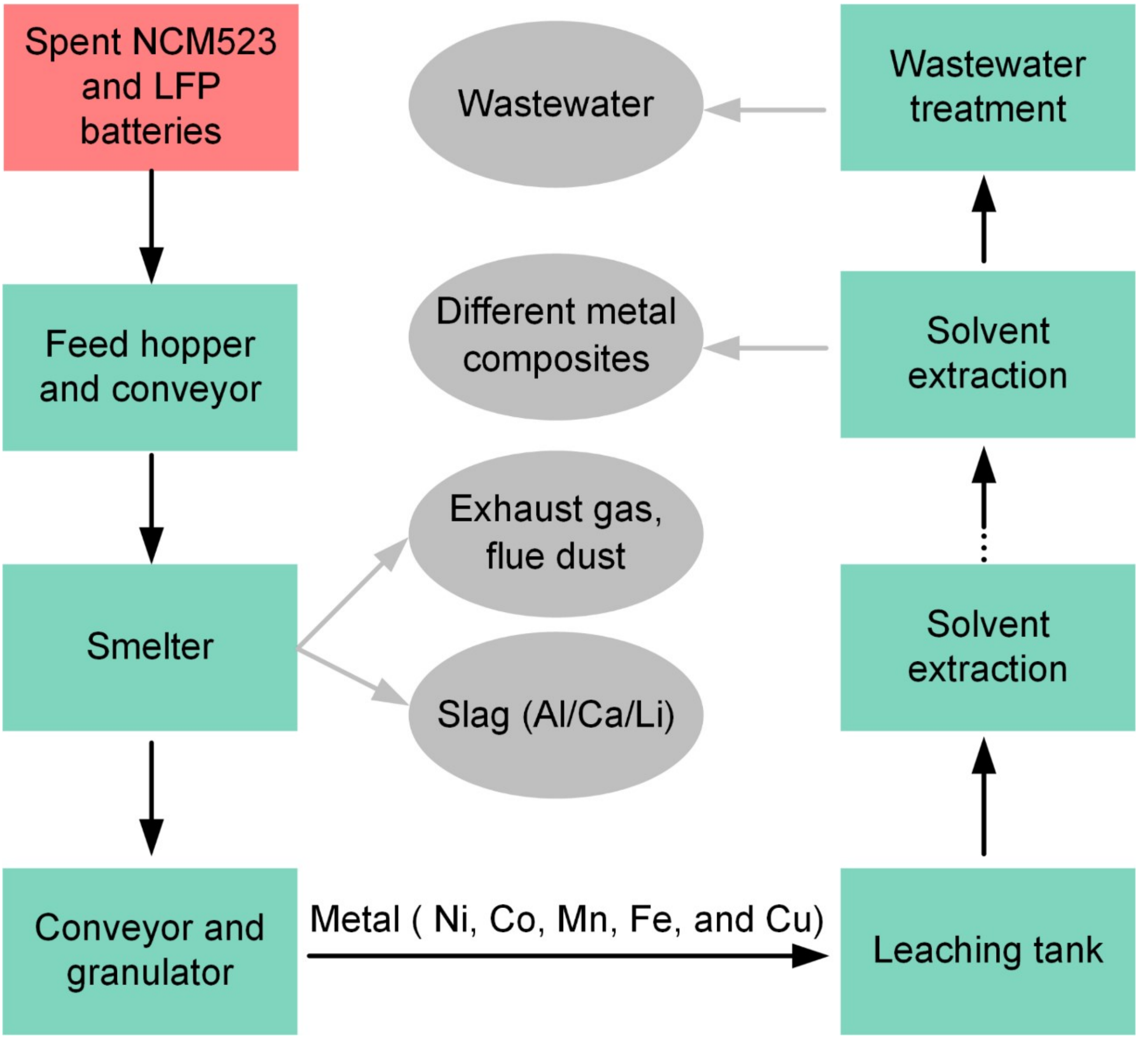

Figure S19 Schematic of Pyro recycling.

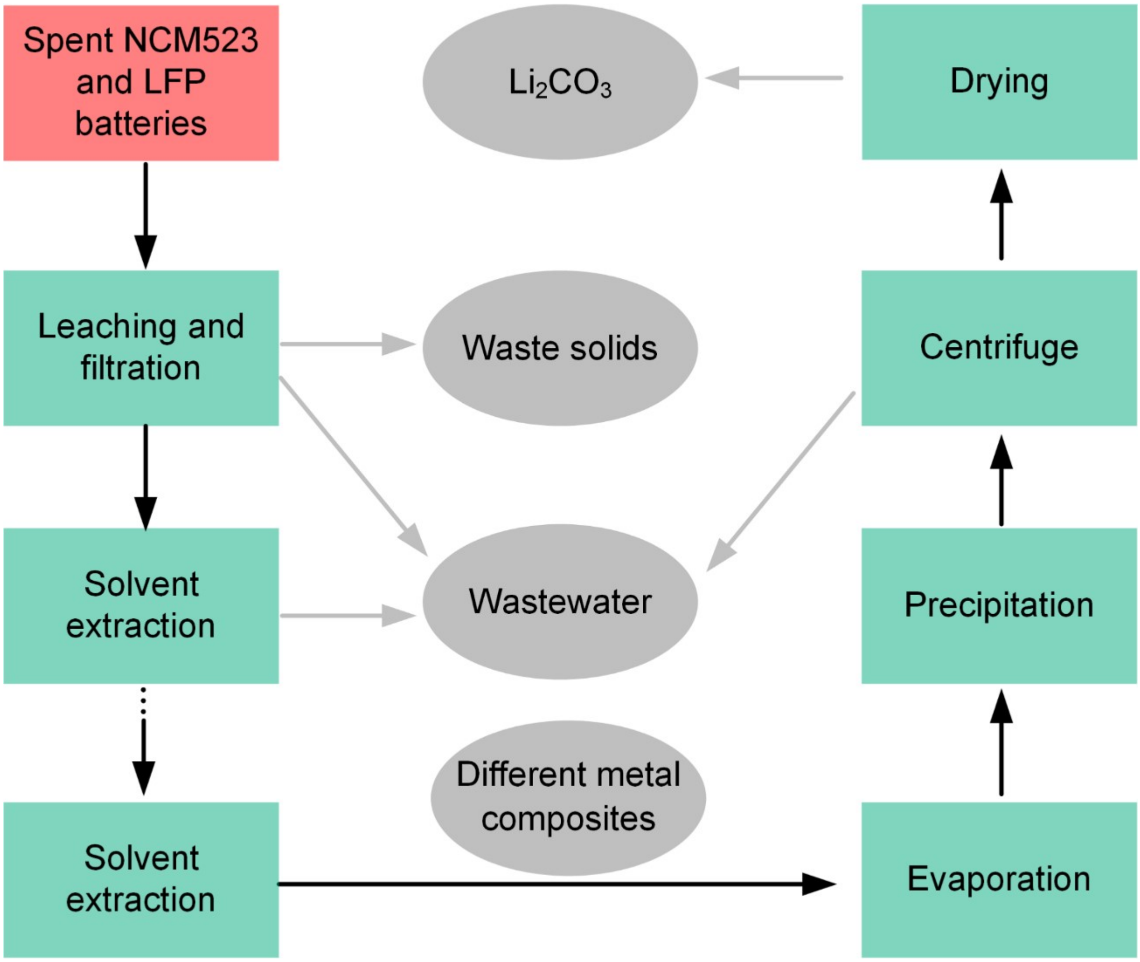

Figure S20 Schematic of Hydro recycling.

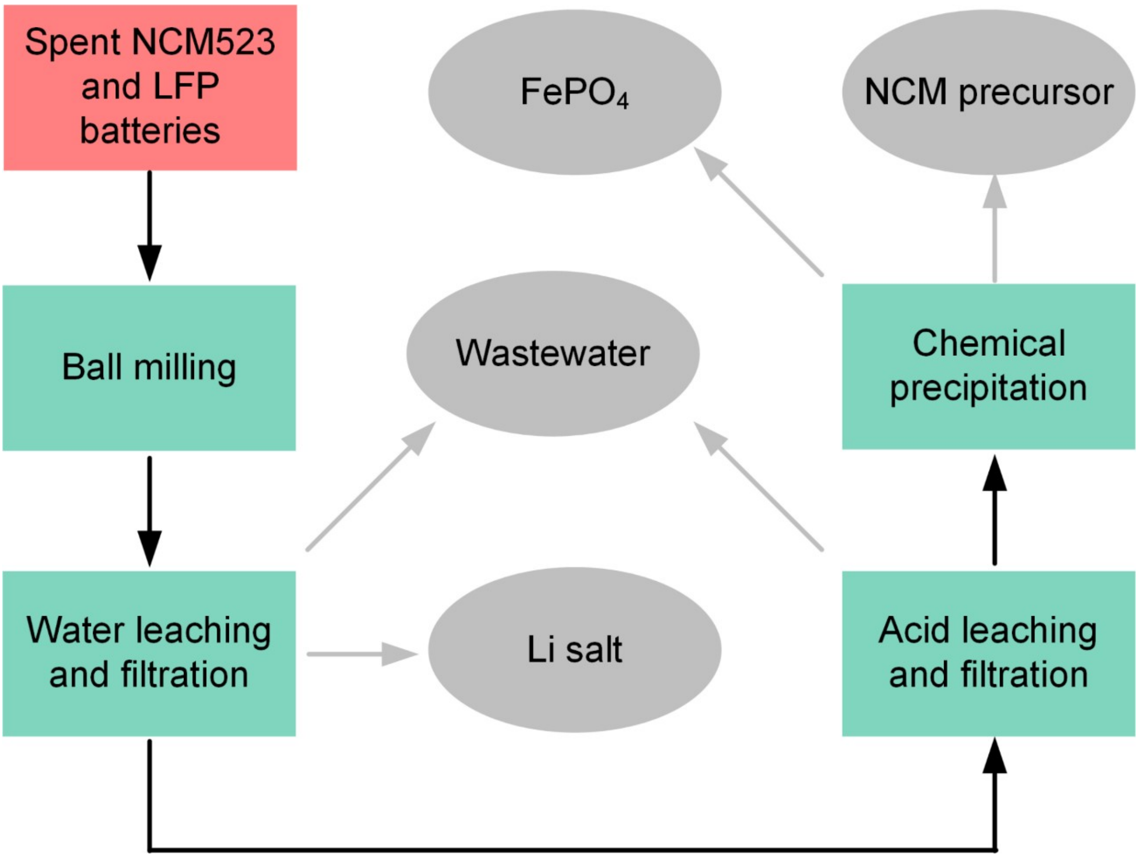

Figure S21 Schematic of this work.

References

[1] A.V. Churikov, A.V. Ivanishchev, A.V. Ushakov, I.M. Gamayunova, I.A. Leenson, Journal of Chemical & Engineering Data, 58 (2013) 1747-1759.
[2] Y. Lixin, in, Lanzhou University of Technology, 2019.
[3] J.A. Dean, Lange's Handbook of Chemistry, New York, 1999.
[4] S.L. Shang, Y. Wang, Z.G. Mei, X.D. Hui, Z.K. Liu, J. Mater. Chem., 22 (2012) 1142-1149.
[5] H. Zhu, Y. Ai, J. Li, J. Min, D. Chu, J. Zhao, J. Chen, Advanced Powder Technology, 22 (2011) 629-633.
[6] P.R. Roberge, Handbook of Corrosion Engineering, New York, 2000.